AIAA JOURNAL
Vol. 32, No. 2, February 1994

Evaluation of Navier-Stokes Solutions Using the Integrated Effect of Numerical Dissipation

R. R. Varma* and D. A. Caughey†
Cornell University, Ithaca, New York 14853

A method for evaluating the quality of solutions to the Navier-Stokes equations is developed and illustrated with representative examples. In solutions to the Navier-Stokes equations it is important that added numerical dissipation does not overwhelm the real viscous dissipation. To verify this, it is necessary to be able to estimate quantitatively the effect of numerical dissipation. A method for estimating the integrated effect of numerical dissipation on solutions to the Navier-Stokes equations is developed in this paper. The method is based on integration of the momentum equations, and the computation of corrections due to numerical dissipation to the drag integral. These corrections can then be considered as estimates of the error due to dissipation. Solutions to the Navier-Stokes equations for laminar and turbulent flows over airfoils are used to illustrate the method. The errors due to numerical dissipation are compared with the total numerical errors in the solutions. The effect of Mach number scaling of the numerical dissipation terms is discussed.

I. Introduction

THE evaluation of the quality of any numerical solution of the Navier-Stokes equations and the validation of the computer code that yielded the solution necessarily require an estimation of the errors in the solution. As Holst[1] has pointed out, these errors fall under two broad categories—physical modeling errors and numerical errors. The physical modeling errors include, among others, those arising from the approximations involved in the Navier-Stokes equations themselves, or their thin-layer approximation, as well as those introduced by any model for the effects of turbulence. The numerical errors include those due to the basic discretization scheme, including any implicit or explicit numerical dissipation, and are dependent upon the fineness and distribution of the grid. Physical modeling errors can be quantified only by comparison with the results of experiments or with the results of direct numerical simulations in which the corresponding approximations are not made. Before these comparisons can be meaningful, however, it is important to understand the level of numerical error, and this can be done without recourse to comparison with experiments. It is with these numerical errors and, in particular, with the effects of numerical dissipation, that the present article is concerned.

The calculation of fluxes in several widely used finite volume schemes used to solve the Euler and Navier-Stokes equations can be shown to be equivalent to central differencing. Such schemes, applied to the Euler equations, do not contain any inherent dissipation. To prevent odd-even point decoupling and oscillations near shock waves or stagnation points, numerical dissipation terms must be added when solving the Euler equations. The Navier-Stokes equations, on the other hand, possess dissipative properties due to the presence of the viscous terms, but the physical dissipation provided by these terms in regions far away from the surface is usually small, and the addition of numerical dissipation terms is still necessary to ensure the stability and robustness of the schemes. While the added dissipation terms must be large enough for this purpose, they must also be small enough not to overwhelm the effects of the real viscous dissipation in regions where the latter is significant.

Most previous attempts at studying the effects of numerical dissipation have been based primarily on qualitative comparisons of computed solutions and experiments. For the Euler equations, Caughey and Turkel[2] looked at the effects upon solution accuracy of various forms of the dissipative terms and the smoothness of the mesh. They used nonphysical behavior of the solution, such as oscillations in the surface pressure distribution near the airfoil trailing edge, to study the effects of numerical dissipation. A similar approach was followed by Swanson and Turkel[3] for both the Euler and Navier-Stokes equations. They analyzed various ways of reducing artificial dissipation in central difference schemes for the solution of these equations. Their efforts were also directed at obtaining better qualitative behavior of the solution in critical regions of the flow and better agreement with experimental data. While this approach provides some useful insight, there is clearly a need to develop a method that provides quantitative estimates of the effect of numerical dissipation on the solution.

In this paper, we first develop a method for estimating quantitatively the integrated effect of numerical dissipation on solutions to the Navier-Stokes equations. Using this method we then evaluate the quality of solutions to the thin-layer Navier-Stokes equations for two-dimensional transonic flows over airfoils obtained using the multigrid diagonal implicit method of Varma and Caughey.[4]

II. Analysis

The governing differential equations considered here are the thin-layer Navier-Stokes equations in two dimensions. These equations are transformed from a Cartesian coordinate system (x, y) into a generalized coordinate system (ξ, η). Near the airfoil surface, the ξ-coordinate is approximately parallel to, and the η-coordinate is approximately normal to, the body. The airfoil surface itself is a ξ-coordinate line. The transformed equations are modified by artificial dissipation terms. The form of dissipation used in these calculations is based on the adaptive blend of second and fourth differences described by Jameson et al.[5] and modified by Caughey.[6] The system of equations can be written in the fully conservative form,

$$\frac{\partial \boldsymbol{W}}{\partial t} + \frac{\partial \boldsymbol{F}}{\partial \xi} + \frac{\partial \boldsymbol{G}}{\partial \eta} - \frac{\partial \boldsymbol{G}'_v}{\partial \eta} - \frac{\partial D_\xi \boldsymbol{w}}{\partial \xi} - \frac{\partial D_\eta \boldsymbol{w}}{\partial \eta} = 0 \tag{1}$$

where

$$\boldsymbol{W} = h\{\rho, \rho u, \rho v, e\}^T \tag{2}$$

Presented as Paper 93-0539 at the AIAA 31st Aerospace Sciences Meeting, Reno, NV, Jan. 11–14, 1993; received April 5, 1993; revision received July 22, 1993; accepted for publication Aug. 3, 1993. Copyright © 1993 by the American Institute of Aeronautics and Astronautics, Inc. All rights reserved.

*Graduate Student; currently Post-Doctoral Fellow, Center for Composite Materials, University of Delaware, Newark, DE 197160. Student Member AIAA.

†Professor and Director, Sibley School of Mechanical and Aerospace Engineering. Associate Fellow AIAA.

is the vector of conserved dependent variables. The transformed inviscid flux vectors are

$$\boldsymbol{F} = h\{\rho U,\ \rho Uu + \xi_x p,\ \rho Uv + \xi_y p,\ (e+p)U\}^T \tag{3}$$

$$\boldsymbol{G} = h\{\rho V,\ \rho Vu + \eta_x p,\ \rho Vv + \eta_y p,\ (e+p)V\}^T \tag{4}$$

Here h is the determinant of the Jacobian of the transformation, ρ is the fluid density, u and v are the respective velocity components in the x and y directions, U and V are the contravariant components of velocity in the ξ and η directions, respectively, and e is the total energy per unit volume. The thin-layer approximation to the transformed viscous flux vector is

$$\begin{aligned}\boldsymbol{G}'_v = h\{&0,\ \eta_x\sigma'_{xx} + \eta_y\sigma'_{xy} + \eta_x\sigma'_{xy} \\ &+ \eta_y\sigma'_{yy},\ \eta_x(u\sigma'_{xx} + v\sigma'_{xy} - q'_x) \\ &+ \eta_y(u\sigma'_{xy} + v\sigma'_{yy} - q'_y)\}^T\end{aligned} \tag{5}$$

where σ'_{xx}, σ'_{xy}, and σ'_{yy} are the thin-layer contributions to the Cartesian viscous stresses, and q'_x and q'_y are the corresponding contributions to the heat fluxes. The dissipative fluxes across cell faces in the ξ and η directions are $D_\xi \boldsymbol{W}$ and $D_\eta \boldsymbol{W}$, where the differential operators D_ξ and D_η have the form

$$D_\xi = \epsilon_\xi^{(2)}\frac{\partial}{\partial\xi} - \frac{\partial}{\partial\xi}\epsilon_\xi^{(4)}\frac{\partial^2}{\partial\xi^2} \quad \text{and} \quad D_\eta = \epsilon_\eta^{(2)}\frac{\partial}{\partial\eta} - \frac{\partial}{\partial\eta}\epsilon_\eta^{(4)}\frac{\partial^2}{\partial\eta^2} \tag{6}$$

The coefficients of dissipation, $\epsilon^{(2)}$ and $\epsilon^{(4)}$, are defined following Caughey.[6]

A. Integration of the Momentum Equations

The analysis that follows is based on a generalized derivation of the Momentum Theorem. The numerical implementation procedure will be discussed in Sec. II.D.2.

Consider a fixed area A bounded by a closed curve C within the computational domain as shown in Fig. 1. The curve C is chosen such that it includes the body surface. Integrating the governing equations [Eq.(1)], which are satisfied at every interior point, over the area A gives

$$\iint_A \left(\frac{\partial \boldsymbol{W}}{\partial t} + \frac{\partial \boldsymbol{F}}{\partial\xi} + \frac{\partial \boldsymbol{G}}{\partial\eta} - \frac{\partial \boldsymbol{G}'_v}{\partial\eta} - \frac{\partial D_\xi \boldsymbol{w}}{\partial\xi} - \frac{\partial D_\eta \boldsymbol{w}}{\partial\eta}\right) d\xi\, d\eta = 0$$

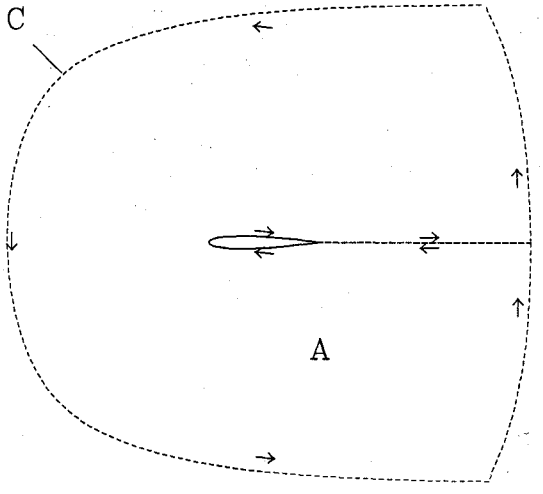

Fig. 1 Contour for integration for drag: closed curve C enclosing area A.

Using Green's theorem, the area integrals over A are converted to line integrals along C. This gives

$$\frac{d}{dt}\iint_A \boldsymbol{W}\, d\xi\, d\eta + \oint_C (\boldsymbol{F}\, d\eta - \boldsymbol{G}\, d\xi) + \oint_C \boldsymbol{G}'_v\, d\xi + \oint_C (D_\eta \boldsymbol{w}\, d\xi - D_\xi \boldsymbol{w}\, d\eta) = 0 \tag{7}$$

At steady state, the first term in Eq. (7) is identically zero, and the integral equation becomes

$$\oint_C [\boldsymbol{F}\, d\eta - \boldsymbol{G}\, d\xi + \boldsymbol{G}'_v\, d\xi + D_\eta \boldsymbol{w}\, d\xi - D_\xi \boldsymbol{w}\, d\eta] = 0 \tag{8}$$

The continuity, the two momenta, and the energy equations have the same integral form. Our interest is restricted to the calculation of drag, and so only the two momentum equations are considered. Before we go on, however, a clarification regarding the notation is required here. As defined by Eqs. (2–5) the vectors $\boldsymbol{W}$, $\boldsymbol{F}$, $\boldsymbol{G}$, and $\boldsymbol{G}'_v$ each have four components corresponding to the four equations. For the rest of this paper, the same vector notation will be used although we consider only the two components corresponding to the momentum equations.

The curve C consists of segments along the body surface, the outer contour, and the branch cut. Continuity of the solution across the cut ensures that all fluxes on one side of the cut exactly equal the corresponding fluxes on the other side. Since the cut is traversed twice—once in each direction—the net integral of fluxes along the cut is zero. Eq. (8) then reduces to a generalized form of the momentum integral equation:

$$\int_{\text{Body}} [\boldsymbol{F}\, d\eta - \boldsymbol{G}\, d\xi + \boldsymbol{G}'_v\, d\xi + D_\eta \boldsymbol{w}\, d\xi - D_\xi \boldsymbol{w}\, d\eta] + \int_{\text{Outer}} [\boldsymbol{F}\, d\eta - \boldsymbol{G}\, d\xi + \boldsymbol{G}'_v\, d\xi + D_\eta \boldsymbol{w}\, d\xi - D_\xi \boldsymbol{w}\, d\eta] = 0 \tag{9}$$

B. Body Surface Integral

The integral over the body in Eq. (9) is further simplified when the mesh on which the solution is obtained is such that the airfoil is a line of constant η as is the case in our calculations. Then, the integral over the body surface reduces to

$$\int_{\text{Body}} (-\boldsymbol{G}\, d\xi + \boldsymbol{G}'_v\, d\xi) + \int_{\text{Body}} (D_\eta \boldsymbol{w}\, d\xi) \tag{10}$$

Using Eqs. (4) and (5), the first term of the above expression can be expanded as

$$\int_{\text{Body}} (-\boldsymbol{G}\, d\xi + \boldsymbol{G}'_v\, d\xi) = \begin{pmatrix} \int_{\text{Body}} [p\, dy - \sigma'_{xx}\, dy + \sigma'_{xy}\, dx] \\ \int_{\text{Body}} [-p\, dx - \sigma'_{xy}\, dy + \sigma'_{yy}\, dx] \end{pmatrix} \tag{11}$$

The physical forces that act on the body, and determine the lift and drag, are caused by pressure and viscous stresses. Expressions for $\mathcal{F}_x$ and $\mathcal{F}_y$, the x and y components respectively of the force $\mathcal{F}$ on the body, can be obtained by integrating the pressure and the viscous stresses. These force components are given by

$$\mathcal{F}_x = \int_{\text{Body}} [p\, dy - \sigma'_{xx}\, dy + \sigma'_{xy}\, dx]$$

$$\mathcal{F}_y = \int_{\text{Body}} [-p\, dx - \sigma'_{xy}\, dy + \sigma'_{yy}\, dx]$$

Therefore, from Eq. (11), we have

$$\int_{\text{Body}} (-\boldsymbol{G}\, d\xi + \boldsymbol{G}'_v\, d\xi) = \mathcal{F} \tag{12}$$

i.e., the integral over the body of the inviscid (pressure) and viscous fluxes acting on the surface gives the net force on the body. Note that the integral over the body surface [Eq. (10)] contains an additional term due to the dissipative fluxes; the significance of this term will be discussed in the following section.

C. Corrected Outer Integral

The momentum integral equation [Eq. (9)] thus yields an expression for the force $\mathcal{F}$ on the body in terms of integrals of the inviscid and viscous fluxes along an outer contour modified by integrals of the numerical dissipation fluxes. From Eqs. (9), (10), and (12), we have

$$\mathcal{F} = \int_{\text{Outer}} (\boldsymbol{G}\, d\xi - \boldsymbol{F}\, d\eta - \boldsymbol{G}'_v\, d\xi)$$

$$+ \int_{\text{Outer}} (D_\xi \boldsymbol{w}\, d\eta - D_\eta \boldsymbol{w}\, d\xi) - \int_{\text{Body}} D_\eta \boldsymbol{w}\, d\xi \tag{13}$$

This is termed the corrected outer integral. It is an equivalent expression for the forces on the body, and consists of contributions from three sources: 1) inviscid contributions from the net pressure forces on the outer contour and the net inviscid momentum flux across it,

$$\int_{\text{Outer}} (\boldsymbol{G}\, d\xi - \boldsymbol{F}\, d\eta)$$

2) contributions from the net viscous stresses acting on the outer contour,

$$\int_{\text{Outer}} (-\boldsymbol{G}'_v\, d\xi)$$

and 3) contributions due to the numerical dissipation which arise from two sources: dissipation fluxes across the outer contour,

$$\int_{\text{Outer}} (D_\xi \boldsymbol{w}\, d\eta - D_\eta \boldsymbol{w}\, d\xi)$$

and dissipation fluxes across the body surface,

$$\int_{\text{Body}} (-D_\eta \boldsymbol{w})\, d\xi$$

If the viscous stresses are negligible on the outer contour and the dissipation terms are absent, then Eq. (13) reduces to the usual form of the momentum integral equation consisting of only the integral of the inviscid fluxes.

The dissipation contributions from the integral over the body can be interpreted as due to artificial sources and sinks of momentum created on the body surface, which lead to an artificial momentum surplus or deficit in the integral along an outer contour. This in turn is reflected in the calculation of forces on the body from such an outer integral. The numerical dissipation contributions listed above may together be considered as corrections due to dissipation to the outer integral for the calculation of the forces $\mathcal{F}_x$ and $\mathcal{F}_y$ on the body, and therefore as corrections also in the calculation of lift and drag.

D. Quantitative Estimates of Dissipation

The added numerical dissipation terms are formally third order in the mesh spacing, and are therefore expected to have very little effect on the solution if the mesh is sufficiently fine. In the calculation of the lift coefficient C_l using the corrected outer integral, the corrections due to dissipation, relative to the inviscid contributions in particular, are expected to be negligible. It is indeed so, as will be shown later. The drag coefficient C_d, on the other hand, is known to be sensitive to small changes in the solution. So we choose to focus our attention on the calculation of the total drag coefficient, C_d(total), on the body.

The two contributions to the body surface integral for drag [from Eq. (12)] are denoted as $C_d(p)$ due to the pressure, and $C_d(f)$ due to the shear stresses on the surface (skin friction). The total drag coefficient is given by

$$C_d(\text{total}) = C_d(p) + C_d(f) \tag{14}$$

For attached flow, we expect the two contributions to be comparable in magnitude. For flows with significant separation, the pressure drag is expected to dominate.

The three contributions to the corrected outer integral for drag [from Eq. (13)] are denoted as C_d(inviscid) due to the pressure and convective terms, C_d(viscous) due to the viscous stresses, and C_d(diss) due to the dissipative fluxes. The total drag coefficient is given by

$$C_d(\text{total}) = C_d(\text{inviscid}) + C_d(\text{viscous}) + C_d(\text{diss}) \tag{15}$$

As described in Sec. II.C, the numerical dissipation flux contributions to the drag coefficient can be separated further into components corresponding to the outer and body-surface contours:

$$C_d(\text{diss}) = C_d(\text{diss-outer}) + C_d(\text{diss-body}) \tag{16}$$

Various contours, at different distances from the surface, are chosen for calculating these contributions to drag. If the body surface is chosen as the outer contour, then we have C_d(diss-outer) $= -C_d$(diss-body), which gives us the body surface integral as expected. For a contour close to the surface, C_d(viscous) is expected to be significant. For contours at sufficiently large distances from the surface, C_d(inviscid) is expected to dominate.

For a steady-state solution, the C_d(total) computed on the surface using the body surface integral [Eq. (14)] must equal exactly the C_d(total) computed along any outer contour using the corrected outer integral [Eq. (15)], since each of these expressions for drag is derived from expressions for $\mathcal{F}$ [Eqs. (12) and (13)] that are exactly equivalent. The addition of the corrections due to dissipation is necessary for this to be true.

1. *Error Due to Dissipation*

Equating the two expressions for C_d(total), we get

$$C_d(\text{total}) = [C_d(p) + C_d(f)]_{\text{Body}}$$
$$= [C_d(\text{inviscid}) + C_d(\text{viscous})]_{\text{Outer}} + C_d(\text{diss})$$

It is clear from this formulation that C_d(diss) values can be considered as errors in the calculation of drag. From among values of C_d(diss) for various possible contours, we choose one which reflects best the error due to numerical dissipation in the solution. It is possible to set C_d(diss-body) to zero through a particular choice of boundary conditions as we shall see in Sec. II.E. Therefore, the value of C_d(diss-body) is not necessarily representative of the total error. Values for C_d(diss-outer) can be calculated for various contours, each value representing the effect of dissipation along that contour. If we want to control the amount of dissipation in the solution, i.e., keep it below a certain level, then the quantity that we should be most concerned about is the maximum value of C_d(diss-outer) along any contour. Therefore, Max[C_d(diss-outer)]is chosen to characterize the error due to dissipation.

2. *Numerical Implementation*

A numerical approximation to the time-dependent equation,

$$\iint_A \left(\frac{\partial \boldsymbol{W}}{\partial t} + \frac{\partial \boldsymbol{F}}{\partial \xi} + \frac{\partial \boldsymbol{G}}{\partial \eta} - \frac{\partial \boldsymbol{G}'_v}{\partial \eta} - \frac{\partial D_\xi \boldsymbol{w}}{\partial \xi} - \frac{\partial D_\eta \boldsymbol{w}}{\partial \eta} \right) d\xi\, d\eta = 0$$

may be satisfied exactly in each cell at each time step according to the discretization procedure. However, in this paper, we will restrict our attention to evaluating the quality of steady-state solutions only. In particular, we will focus on the solutions obtained using the multigrid method described by Varma and Caughey.[4] The criterion for convergence to the steady state is that the residuals of the equations be reduced to values below a certain level. If the numerical solution is converged such that the residuals are down to round-off levels, then the steady state equation [(Eq. 8)]

$$\oint_C [\boldsymbol{F}\, d\eta - \boldsymbol{G}\, d\xi + \boldsymbol{G}'_v\, d\xi + D_\eta \boldsymbol{w}\, d\xi - D_\xi \boldsymbol{w}\, d\eta] = 0 \qquad (17)$$

is satisfied to machine precision in each cell. This equation is also satisfied for a curve C enclosing several cells, such as shown in Fig. 1, if the numerical scheme is conservative in transport and therefore globally conservative, and the fluxes across the curve are calculated in a manner which is consistent with the way they are evaluated in the residual calculation in the iterative solver. The calculation of these fluxes is greatly simplified if the curve C is chosen along grid lines. In this case, the total flux is taken to be the sum of the fluxes, as computed by the iterative flow solver, across the individual cell faces that make up the curve. It follows that the value of C_d (total) evaluated on the body surface using the body surface integral [Eq. (14)] must agree with the value calculated along any outer contour using the corrected outer integral [Eq. (15)] to within the degree of convergence.

E. Dissipation Schemes

The analytical form of the adaptive blend of second and fourth difference dissipation is given by Eq. (6). Numerical implementation of this form of dissipation requires the specification of boundary conditions on both the second and fourth difference terms. Along the cut the conditions are periodic, and in the far field the gradients are assumed to be negligible. However, on the body surface, boundary conditions for the normal dissipative flux,

$$D_\eta \boldsymbol{w} = \epsilon_\eta^{(2)} \frac{\partial \boldsymbol{w}}{\partial \eta} - \frac{\partial}{\partial \eta} \epsilon_\eta^{(4)} \frac{\partial^2 \boldsymbol{w}}{\partial \eta^2}$$

cannot be specified uniquely based on simple physical reasoning. Several different implementations of the boundary conditions on the normal dissipation fluxes are discussed by Varma and Caughey.[7] Those that lead to nonzero numerical dissipation fluxes on the body surface yield poor quality solutions near the surface, particularly on the coarser grids. In this paper, we will consider two implementations:

1) Scheme A: The numerical dissipation fluxes—both the first and third difference fluxes—on the solid surface are set equal to zero. This leads to

$$(D_\eta \boldsymbol{w})_{i,1^1/_2} = 0$$

Therefore, only the real viscous and inviscid fluxes are nonzero on the body surface.

2) Scheme B: In regions of large gradients, such as the boundary layer and the wake, the numerical dissipation fluxes are expected to be large. But these are the very regions where the viscous effects are also important. Therefore, in viscous calculations it is common to scale the numerical dissipation in the normal direction by multiplying the fluxes by some function of the local Mach number. This technique is expected to reduce the effect of numerical dissipation near the surface where the local Mach numbers are low without affecting it in the rest of the flowfield.[8] Here the η-direction numerical dissipation fluxes across cell faces parallel to the ξ-direction are scaled by the local Mach number normalized by the freestream Mach number, i.e.,

$$D_\eta \boldsymbol{w} = f(M) \times \left(\epsilon_\eta^{(2)} \frac{\partial \boldsymbol{w}}{\partial \eta} - \frac{\partial}{\partial \eta} \epsilon_\eta^{(4)} \frac{\partial^2 \boldsymbol{w}}{\partial \eta^2} \right)$$

where $f(M) = M/M_\infty$.

Table 1 Contributions to drag coefficient due to inviscid fluxes, viscous fluxes, dissipation fluxes along the outer contour, and dissipation fluxes across the body surface, and total drag coefficient for four choices of contours: laminar case, 256 × 72 grid, scheme A

Distance from body (chords)	C_d (inviscid)	C_d (viscous)	C_d (diss-outer)	C_d (diss-body)	C_d (total)
0 [body]	232	352	—	—	584
2.7×10^{-4}	244	348	−8	0	584
5.2×10^{-3}	354	199	31[a]	0	584
1.0	584	≈0	≈0	0	584

[a]Denotes maximum value of C_d (diss-outer)

Table 2 Comparison of numerical error and dissipation error estimates—turbulent flow cases, scheme A

	Grid size	$C_d(f)$	$C_d(p)$	Error in $C_d(p)$	Diss error
Turbulent case 1	128 × 36 (4h)	65.9	52.7	26.7	39.6
	256 × 72(2h)	63.5	31.7	5.7	15.7
	512 × 144 (h)	62.2	27.4	1.4	4.5
	$h \to 0$	61.8	26.0	—	—
Turbulent case 2	128 × 36 (4h)	66.1	216.0	21.9	40.9
	256 × 72 (2h)	62.8	199.7	5.6	12.9
	512 × 144 (h)	61.9	195.4	1.3	3.3
	$h \to 0$	61.6	194.1	—	—

F. Total Numerical Error

Estimates of the total numerical error in the solution can be obtained using Richardson extrapolation.[9] Given an initial grid, coarser grids are obtained successively by removing every other line in each of the two coordinate directions. Iteratively converged solutions are first computed on the finest grid (denoted by the subscript h), and then on two successively coarser grids (denoted by subscripts $2h$ and $4h$). The coefficient of total drag C_d and contributions due to skin friction and pressure forces are computed on each of these grid levels. Asymptotic values (denoted by subscript 0), i.e., values in the limit of zero mesh spacing, are estimated based on the order of convergence. When the convergence is second order, as expected for the computational scheme used here, the estimate of the asymptotic value is $(C_d)_0 = {}^1/_3 [4(C_d)_h - (C_d)_{2h}]$. Convergence studies for the drag coefficient to be presented in the next section verify this second-order accuracy. From the asymptotic values, the total numerical errors in the drag coefficient for each grid level can be calculated.

III. Results of Solution Evaluations

Representative laminar and turbulent flow solutions to the Navier-Stokes equations for flows past airfoils are evaluated using the method described in the preceding section. In the two lifting cases analyzed here, the effect of the numerical dissipation on the lift coefficient is found to be negligible—less than 0.1% on all grids. However, the effect of the dissipation on the drag coefficient is not negligible. And so, as mentioned earlier, we will concentrate on the precise calculation of the drag coefficient.

For each calculation, the coefficient of drag is computed using the body surface integral and corrected outer integrals. From a breakdown of contributions to the computed drag along various contours, the error due to numerical dissipation is estimated quantitatively. The asymptotic behavior of this error is studied as the grid is refined. The estimated dissipation error is compared with the total numerical error, which is obtained using Richardson extrapolation. This procedure is repeated for the two numerical dissipation schemes described in Sec. II.E, and the merits of the schemes are discussed. The usefulness of this method in evaluating the quality of flow solutions is thus demonstrated.

Table 3 Error due to numerical dissipation—scheme A

	Grid size	Dissipation error	C_d(total)
Laminar case	128 × 36 (4*h*)	121.9	630.8
	256 × 72 (2*h*)	30.8	584.3
	512 × 144 (*h*)	4.6	569.8
Turbulent case 1	128 × 36 (4*h*)	39.6	118.6
	256 × 72 (2*h*)	15.7	95.2
	512 ×144 (*h*)	4.5	89.5
Turbulent case 2	128 × 36 (4*h*)	40.9	282.0
	256 × 72 (2*h*)	12.9	261.1
	512 × 144 (*h*)	3.3	256.5

All values for the coefficient of drag in the tables presented here are expressed in terms of drag counts; one drag count equals 0.0001.

A. Representative Solutions

Three different flow solutions—one laminar case and two turbulent cases—are evaluated.

We first evaluate the laminar case—NACA 0012 airfoil at M_∞ = 0.5, α = 0 deg, and Re_∞ = 5000. This is a symmetric airfoil at zero angle of attack; consequently the lift is zero. The coefficient of drag is therefore computed from the integral of the x-momentum equation alone

We then evaluate turbulent case 1—NACA 0012 airfoil at M_∞ = 0.7, α = 1.49 deg, and $Re_\infty = 9 \times 10^6$. The solutions computed for this case indicate that the flow is attached and is only slightly supersonic in a small pocket near the leading edge on the upper surface. Therefore the pressure drag is relatively small, and the skin-friction drag is a significant portion of the total drag.

Finally, we evaluate turbulent case 2—RAE 2822 airfoil at M_∞ = 0.75, α = 2.5 deg, and $Re_\infty = 6.2 \times 10^6$. The computed solutions show a strong shock above the airfoil at about 65% of the chord producing wave drag and causing a significant amount of flow separation. The pressure drag component, and therefore the total drag, is substantially larger than in the NACA 0012 case.

Well-converged solutions were computed using the MDI algorithm[4] with Schemes A and B for the numerical dissipation (Sec. II.E). The finest grids (512 × 144) used in the series of calculations presented here were generated using the GRAPE program.[10] For the laminar flow calculations, the distance to the first grid point normal to the airfoil surface was about 10^{-4} chord; while for the turbulent flow calculations, it was about 10^{-6} chord. For all three grids, 62.5% of the mesh cells in the wrap-around direction were on the airfoil surface. From each fine grid two coarser grids (256 × 72 and 128 × 36) were obtained sequentially by removing every other line in each of the two mesh directions. The coarsest grid was fine enough to resolve most features in the boundary layer.

B. Dissipation Error Estimates

The estimation of dissipation errors is demonstrated using Scheme A for the laminar flow solution obtained on the 256 × 72 grid. (See Table 1.) The body surface integral is used to obtain the pressure and skin-friction drag components on the airfoil surface. The pressure drag [$C_d(p)$ = 0.0232] accounts for about 40% of the total drag; the skin-friction component [$C_d(f)$ = 0.0352] accounts for the remaining 60%. The contributions to the total drag computed using the corrected outer integral along two outer contours—one close to the surface and the other about a chord away—are considered next. The breakdown of C_d into its various components is as expected. Along a contour corresponding to the first gridline off the surface (2.7×10^{-4} chord), the breakdown of C_d between the inviscid and viscous components is still roughly 40:60. But there is a correction due to dissipation [C_d(diss) = −0.0008] which is about 1.4% of the total drag. Along a contour which is a chord away from the surface, the inviscid flux integral [C_d(inv) = 0.0584] essentially gives the total drag. Because we set the numerical dissipation fluxes on the surface to zero, the correction due to dissipation C_d(diss) is solely from the outer integral of the dissipation fluxes. The maximum value of C_d(diss-outer), which occurs along a contour about 0.005 chord from the airfoil surface, is about 0.0031. This value amounts to about 5.3% of the total drag coefficient, and provides an estimate of the error due to dissipation in the solution. As expected for an iteratively converged solution, the total drag coefficient has the same value of 0.0584 for all contours, including the body surface. In this manner, dissipation error estimates—maximum values of C_d(diss-outer)—are easily obtained for all solutions.

The asymptotic behavior of the dissipation errors as the grid is refined is studied next. Table 2 shows the dissipation errors and the total drag coefficients on the three grid levels for the three cases. As expected, the dissipation errors are relatively large (14–33% here) on the coarsest grids and small (only up to 5% here) on the finest grids. For the laminar case, the dissipation error goes down by a factor of about four from the coarsest grid to the next finer grid, and by a factor of nearly seven from the latter grid to the finest grid. For the two turbulent-flow cases, the dissipation errors on the finer grids reduce only by a factor of about four. The dissipation terms introduce third-order errors for a uniform grid. The reduced accuracy seen here may be due to the stretching of the grid, particularly in the boundary layer.

C. Comparison of Total and Dissipation Errors

The total numerical errors in the solutions can be estimated using Richardson extrapolation. To obtain these estimates, the values of the pressure drag $C_d(p)$ and the skin-friction drag $C_d(f)$ on the three grid levels are considered. The order of convergence of the drag components is determined, and the errors estimated from the asymptotic values. Comparisons for the two turbulent-flow cases are presented here.

The solutions for the turbulent case 1 are analyzed first. The skin-friction drag values, as seen in Table 3, are quite close to the asymptotic value of 0.00618 even on the coarse meshes. To estimate the total numerical errors in the solutions, we will consider the $C_d(p)$ values. The convergence of $C_d(p)$ in the limit as the square of the mesh spacing tends to zero is shown in Fig. 2. The line indicates the linear least-squares fit for the data points corre-

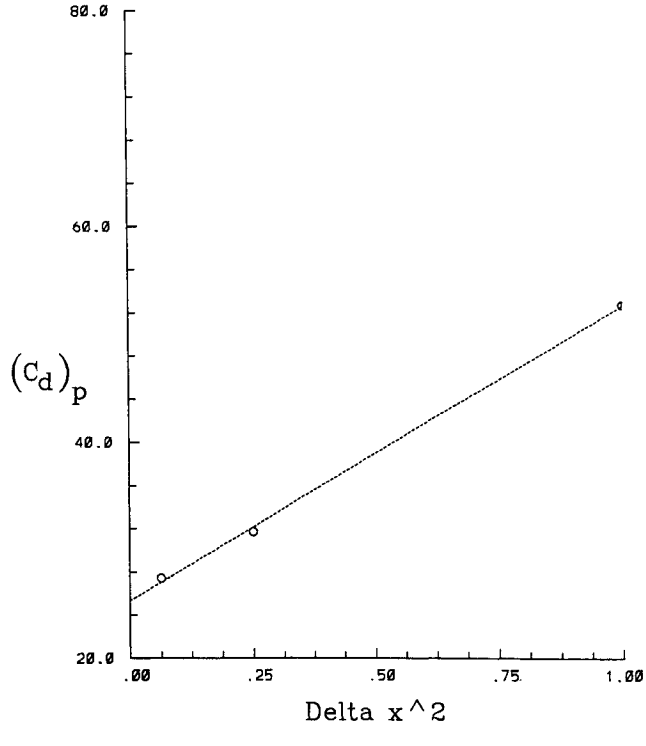

Fig. 2 Plot showing the pressure drag components on meshes with spacings *h*, 2*h*, and 4*h*; and the linear least squares fit through them—turbulent case 1, Scheme A (Table 3).

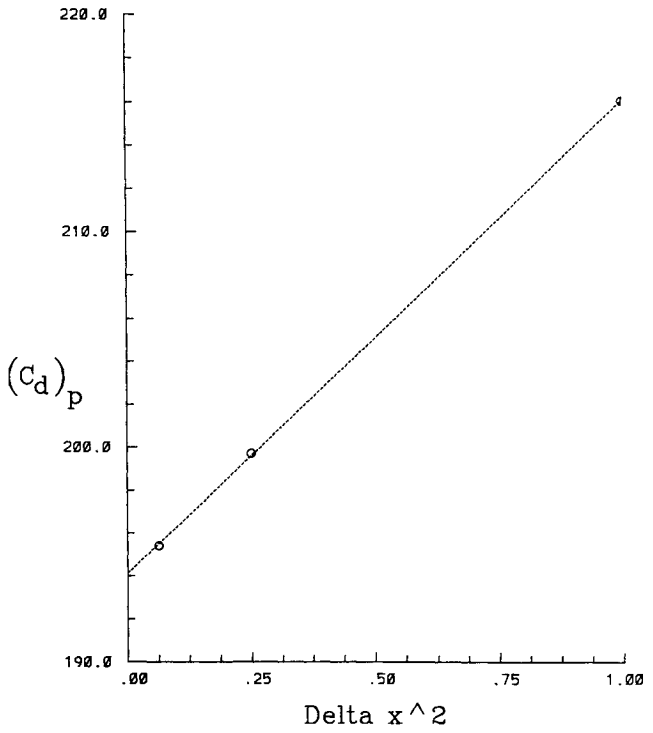

Fig. 3 Plot showing the pressure drag components on meshes with spacings h, $2h$, and $4h$; and the linear least squares fit through them—turbulent case 2, Scheme A (Table 3).

sponding to the three grids. The convergence is close to second-order accurate. The asymptotic value for the pressure drag—$C_d(p)$ = 0.0026—is calculated. The errors in $C_d(p)$ are computed and compared with the errors due to dissipation in Table 3. The two errors are of comparable magnitude on all three grids, although the dissipation errors are consistently larger than the total numerical error estimates.

The turbulent case 2 solutions are considered next. The values of $C_d(f)$ are fairly accurate even on the coarse meshes as seen in Table 3; an asymptotic value of about 0.0062 is estimated. The computed pressure drag, which is affected by the strength of the shock and the extent of flow separation, depends more strongly on the resolution of the grid. The values of $C_d(p)$ on the three grids are shown in Table 3, and are plotted against the square of the mesh spacing in Fig. 3. The convergence is again very nearly second-order accurate; an asymptotic value for $C_d(p)$ equal to 0.0194 is obtained. Based on this asymptotic value, errors in $C_d(p)$, which can also be considered as estimates of the total numerical error in the solutions, are computed. Comparison of these errors with the errors due to dissipation shows again that the two are of comparable magnitude but the dissipation errors are larger than the estimated numerical errors on all grid levels.

D. Mach Number Scaling of Dissipation Terms

Solutions for the three representative cases computed with and without Mach number scaling of the dissipation terms are analyzed and compared in this section. In Scheme A, the dissipation fluxes on the surface are set to zero and therefore C_d(diss-body) is identically zero. In Scheme B, the dissipation fluxes in the η-direction were scaled by the local Mach number normalized by the free-stream Mach number. The local Mach number on the airfoil surface is zero because of the no-slip boundary condition, so the numerical dissipation fluxes on the surface are again identically zero.

The pressure and skin-friction drag components for the laminar flow case on the three grids are compared for Schemes A and B in Fig. 4. For each of the drag components, the asymptotic values as the mesh spacing tends to zero are nearly the same for both schemes [$C_d(p)$ = 0.0232–0.0233; $C_d(f)$ = 0.0332–0.0334]. On the finest grid, the two solutions are very similar because the dissipation errors are very small. The drag component values for both schemes are essentially second-order accurate. However, the values with Mach number scaling are closer to the asymptotic values.

The errors due to numerical dissipation in the total drag coefficients for the two schemes are compared next. The results for the laminar flow case are shown in Fig. 5. At the finest grid level, the dissipation error in Scheme B is only slightly less than in the other schemes, but on the coarser meshes the effect of the Mach number scaling of the dissipation terms appears more significant. The results for one of the turbulent flow cases (turbulent case 2) are shown in Fig. 6. The errors range from about 15% of the total drag on the coarsest grid to about 1% on the finest grid. They appear to approach third-order accuracy on the finer grids. For both schemes the dissipation errors are of comparable magnitude, but a reduction in the dissipation error with Mach number scaling is observed.

E. Summary of Results

For three cases involving both laminar and turbulent flows, the errors due to numerical dissipation are estimated and compared with the total numerical error. The total numerical errors are based on the errors in the drag components, while the dissipation errors

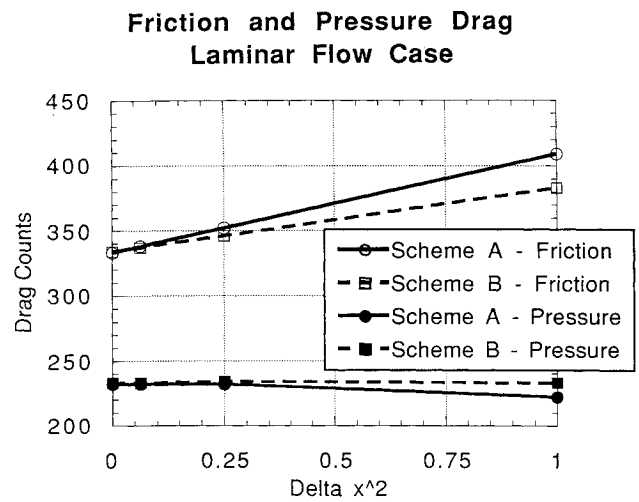

Fig. 4 Convergence with mesh spacing of the pressure and skin-friction drag coefficients for Schemes A and B—laminar case.

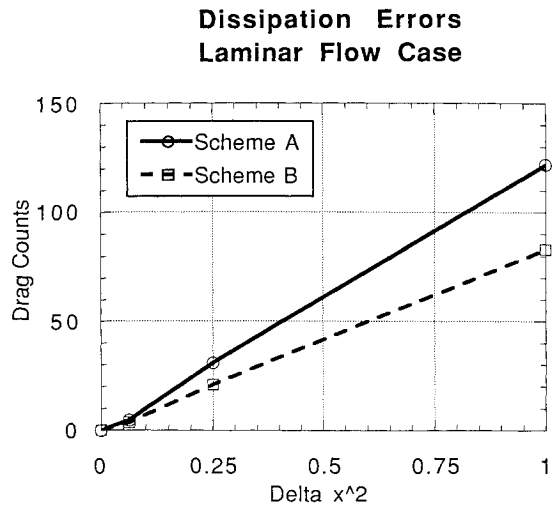

Fig. 5 Reduction in dissipation error with mesh spacing for Schemes A and B—laminar case.

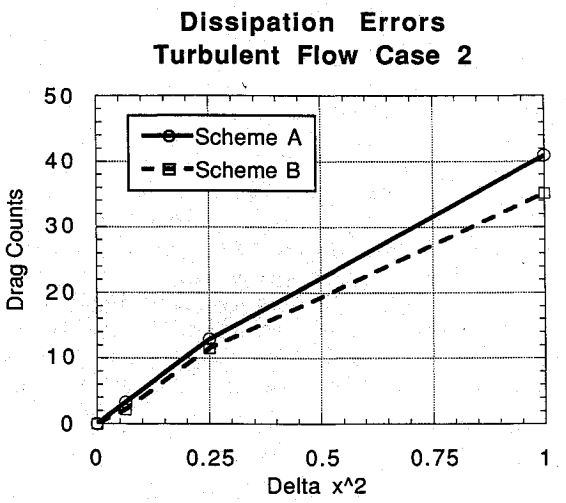

Fig. 6 Reduction in dissipation error with mesh spacing for Schemes A and B—turbulent case 2.

are based on the maximum value of C_d(diss-outer). In the cases considered here, the two errors are of the same order of magnitude, although the dissipation errors are in general larger than the total numerical errors. The total numerical errors scale very nearly with the second power of the grid spacing, but the dissipation errors are consistently between second and third order, even on rather fine grids. Both schemes for numerical dissipation produce errors of comparable magnitude in all cases. However, the Mach number scaling of the dissipation terms reduces the dissipation errors in most cases.

IV. Conclusions

A method for estimating the effect of numerical dissipation on solutions to the Navier-Stokes equations is developed. The analysis follows a generalized derivation of the momentum integral equations. An exact expression for the lift and drag forces on a body is obtained in terms of a corrected outer integral. This integral contains corrections due to dissipation in addition to contributions from inviscid and viscous fluxes along the outer contour. The results presented here demonstrate that the corrections to drag due to the added numerical dissipation can be used to estimate the effect of this dissipation on the solution. The total numerical error can be estimated using Richardson extrapolation from the values of the pressure and skin-friction drag on the surface. These two error estimates together provide a means of judging the quality of computed solutions. The dissipation errors and the total numerical errors are of comparable magnitude for the cases considered here. While the total numerical errors are second order in the mesh spacing as expected, the dissipation errors are between second and third order. Mach number scaling of the normal numerical dissipation fluxes reduces the dissipation errors in most cases.

As Navier-Stokes computations for high Reynolds number flows become more routine, the need for better techniques for evaluating the quality of the solutions becomes more important. The dissipation error estimation method described here is a useful tool for this purpose. It can also be used to guide the development of new numerical dissipation models.

Acknowledgments

This work was supported in part by the NASA Ames Research Center under grant NAG 2-665. The calculations reported here were performed at the Cornell National Supercomputer Facility, a resource of the Cornell Theory Center, which receives major funding from the National Science Foundation and the IBM Corporation, with additional support from New York State, and the Corporate Research Institute.

References

[1]Holst, T. L., "Viscous Transonic Airfoil Compendium of Results," *Journal of Aircraft*, Vol. 25, No. 12, 1988, pp. 1073–1087.

[2]Caughey, D. A., and Turkel, E., "Effects of Numerical Dissipation on Finite-Volume Solutions of Compressible Flow Problems," AIAA Paper 88-0621, Jan. 1988.

[3]Swanson, R. C., and Turkel, E. "Artificial Dissipation and Central Difference Schemes for the Euler and Navier-Stokes Equations," AIAA Paper 87-1107, June 1987.

[4]Varma, R. R., and Caughey, D. A., "Diagonal Implicit Multigrid Solutions of Compresible Turbulent Flows, AIAA Paper 91-1571, June 1991.

[5]Jameson, A., Schmidt, W., and Turkel, E., "Numerical Solutions of the Euler Equations by Finite Volume Methods Using Runge-Kutta Time-Stepping Schemes," AIAA Paper 81-1259, June 1981.

[6]Caughey, D. A., "Diagonal Implicit Multigrid Algorithm for the Euler Equations," *AIAA Journal*, Vol. 26, No. 7, 1988, pp. 841–851.

[7]Varma, R. R., and Caughey, D. A., "Evaluation of Navier-Stokes Solutions Using the Integrated Effect of Numerical Dissipation," AIAA Paper 93-05393, Jan. 1993.

[8]Kaynak, U., and Flores, J., "Advances in the Computation of Transonic Separated Flows Over Finite Wings," AIAA Paper 87-1195, June 1987.

[9]Ferziger, J. H., *Numerical Methods for Engineering Application*, Wiley-Interscience, New York, 1981.

[10]Sorenson, R. L., "A Computer Program to Generate Grids about Two-Dimensional Airfoils and Other Shapes by the Use of Poisson's Equation," NASA TM-81198, 1980.